Science Advances
AAAS

advances.sciencemag.org/cgi/content/full/6/24/eaba6012/DC1

Supplementary Materials for

Real-time detection of single-molecule reaction by plasmon-enhanced spectroscopy

Chao-Yu Li, Sai Duan, Jun Yi, Chen Wang, Petar M. Radjenovic, Zhong-Qun Tian, Jian-Feng Li*

*Corresponding author. Email: li@xmu.edu.cn

Published 10 June 2020, *Sci. Adv.* **6**, eaba6012 (2020)
DOI: 10.1126/sciadv.aba6012

This PDF file includes:

Text S1
Figs. S1 to S11

Text S1. The detailed description of the functionalization process of RITC molecules on the substrate surface via isothiocyanate-amino reaction.

In this work, the dye molecules are covalently functionalized onto the surface through isothiocyanate-amino chemistry (*49*). The number of dyes attached on the surface is controlled by both NH_2 group density and concentration of rhodamine B isothiocyanate (RITC), as shown in fig. S1. In detail, this purpose was accomplished via two steps:

1. Modification of NH_2 group onto SiO_2 surface.

To obtain an extremely low concentration of dyes on surface, an amino density of 1‰ was achieved by using a mixture of triethoxypropylsilane (TEPS) and aminopropyltriethoxysilane (APTS), where the TEPS/APTS ratio is ~1000/1 (vol/vol). It has been reported that the density of amine group of silane monolayer is ~3 nm^{-2} (*50*), which indicates the number density of NH_2 group in our work was ~ 0.003 nm^{-2}.

2. Functionalization of RITC onto surface via isothiocyanate-amino reaction

RTIC molecule has a terminal isothiocyanate (N=C=S) group, which can react with an amine compound (a nucleophile), such as APTS, to form an isothiourea bond. In addition, a small amount of *N, N*-diisopropylethylamine (DIPEA) was added to maintain a weak alkaline environment, where the amino groups are mainly unprotonated. This isothiocyanate-amino reaction is one of the classic protocols in bioconjugation, which has been widely used for functionalizing silica surface and labeling proteins with fluorescent probes (*49*). Therefore, RITC was covalently functionalized onto the surface via isothiocyanate-amino reaction with APTS. The thiourea linkage, the covalent bond between RITC and amino group, is strong enough to prevent diffusion of RITC under the experimental conditions.

On the other hand, in the cases of non-covalent bond RITC (e.g. hydrogen bond or physical absorption), the interactions are weak and the molecules may diffuse on the surface. However, in this work, substrate was thoroughly washed with high polarity solvent (e.g. ethanol), to guarantee the removal of the undesirable weakly adsorbed RITC molecules. Therefore, the RTIC dyes remained on the substrate were stably anchored on the silica surface through the covalent isothiourea bond, which is important for our single-molecule experiment.

Because a nanomolar concentration of dye is typically used for single-molecule spectroscopy (*6*, *20*), a ~0.02-0.1 nM RITC ethanol solution was then used for the functionalization of fluorescent probe onto surface. Considering side reactions and reactant loss under such ultra-low concentration

conditions, the yield of the isothiocyanate-amino reaction is assumed to ~50% (the possible losses induced by the absorption of dyes onto the back and sides of Si(111) wafer substrate is not considered). In this work, a 2.5 cm × 2.5 cm wafer substrate was immersed in a RITC bulk solution (~3 mL), the number density of RITC on the nanocavity substrate is ~3-14 × 10^{-5} dyes per square nanometer for a dye solution concentration of ~0.02 to 0.1 nM.

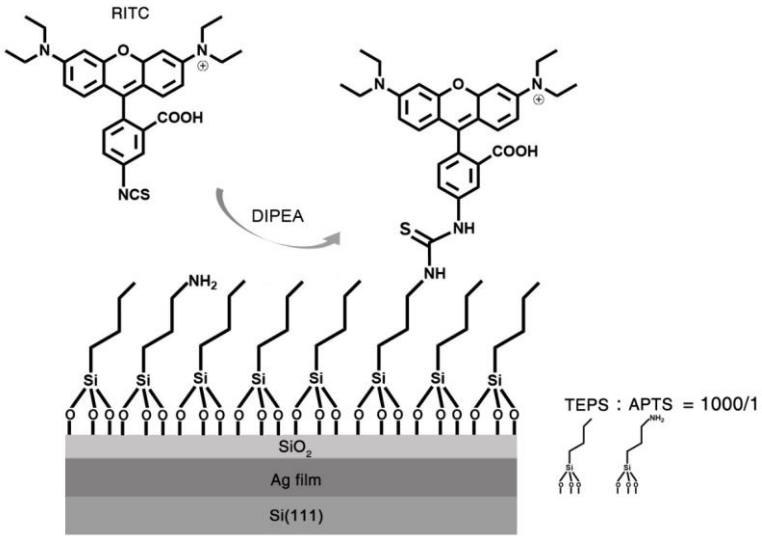

fig. S1. Schematic of the dye-functionalization process.

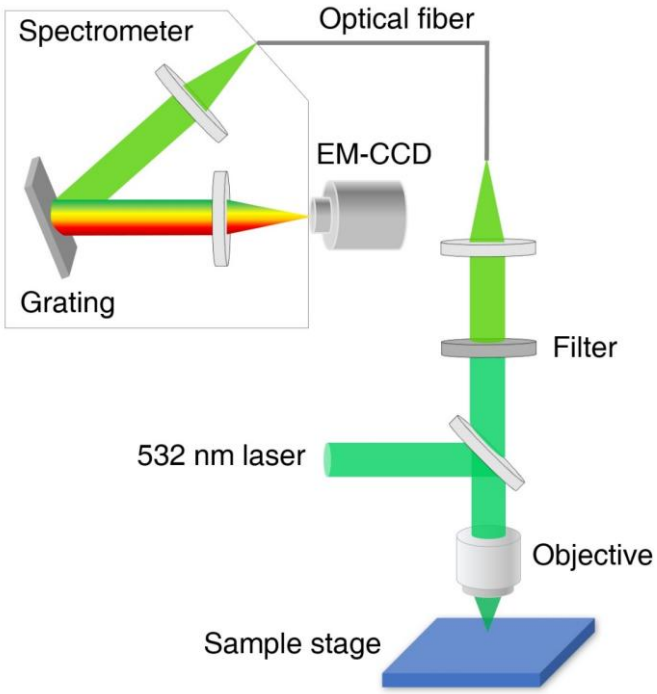

fig. S2. Experimental set-up for SM spectroscopy.

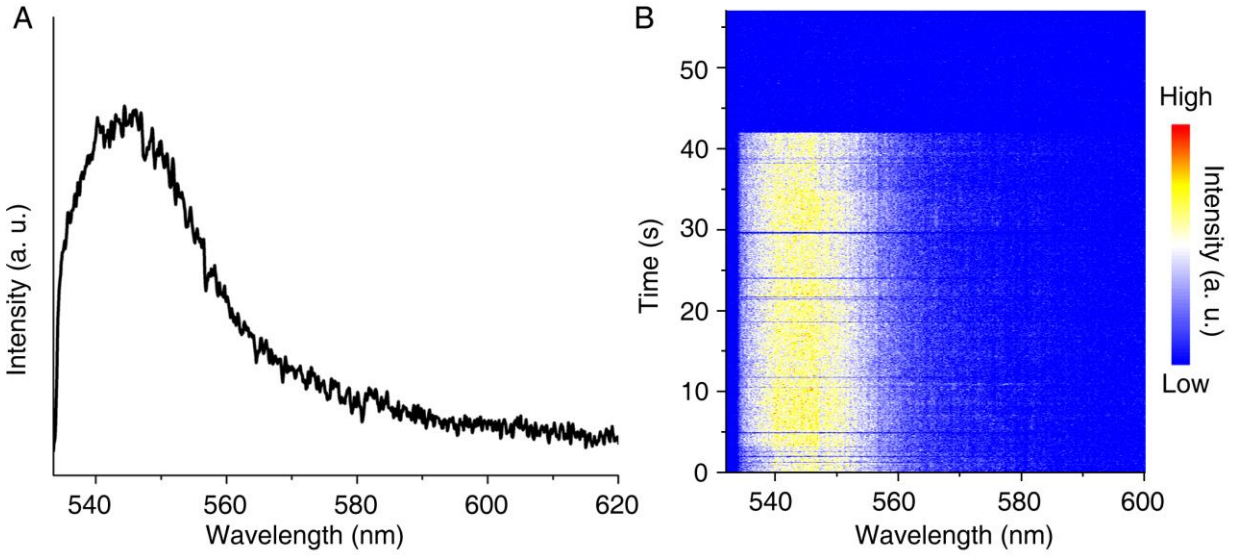

fig. S3. Representative plasmon-enhanced SM fluorescence emission spectroscopy of RITC. (A) Average Plasmon-enhanced SM fluorescence emission spectrum of a single RITC molecule in a nanocavity substrate constructed with the 10-nm shell Ag SHINs. The SM event corresponds to the intensity trajectory shown on the right of Fig. 1A. (**B**) Corresponding color-coded contour plot of time-dependent emission spectra, spectral acquisition time = 50 ms. For a higher SNR, a Savitzky-Golay filter was used to smooth the spectra.

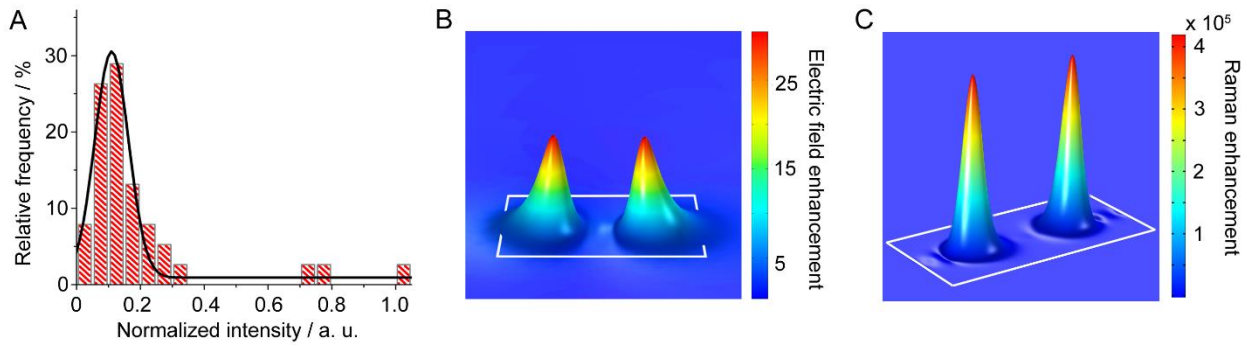

fig. S4. Intensity distribution and enhancement simulations of single-molecule spectroscopy on 10-nm shell Ag SHINs substrate. (**A**) Emission intensity distribution of SM spectroscopy using10-nm shell Ag SHINs substrate, where the black curves represent the Gaussian fit. (**B**) and (**C**), Simulated electric field and Raman enhancement distributions of 10-nm shell Ag SHINs substrate using FEM calculation.

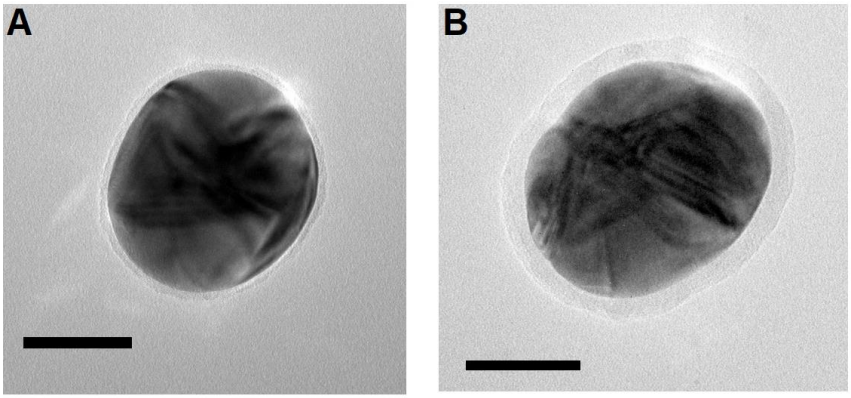

fig. S5. High-resolution transmission electron microscopy (HR-TEM) characterization of SHIN. HR-TEM images of Ag SHIN with (**A**) 2-nm and (**B**) 10-nm silica shell. The scale bars in both A and B are 50 nm.

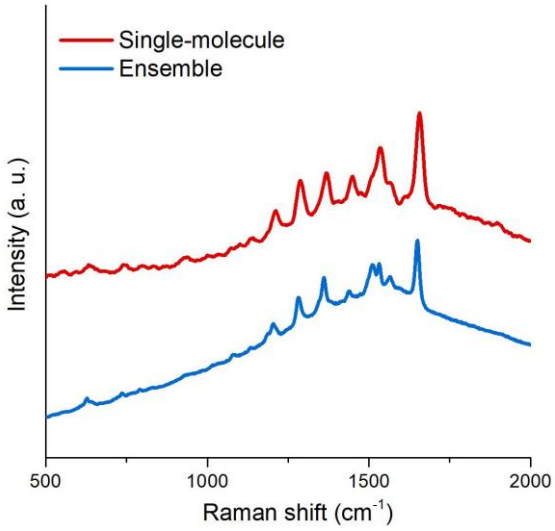

fig. S6. Comparison between plasmon-enhanced emission spectra of a single RITC molecule and ensemble RITC. Plasmon-enhanced emission spectrum of a single RITC molecule (red curve) and ensemble RITC (blue curve). SM spectrum corresponds to the data shown in Fig. 2D. The intensities have been scaled for comparison.

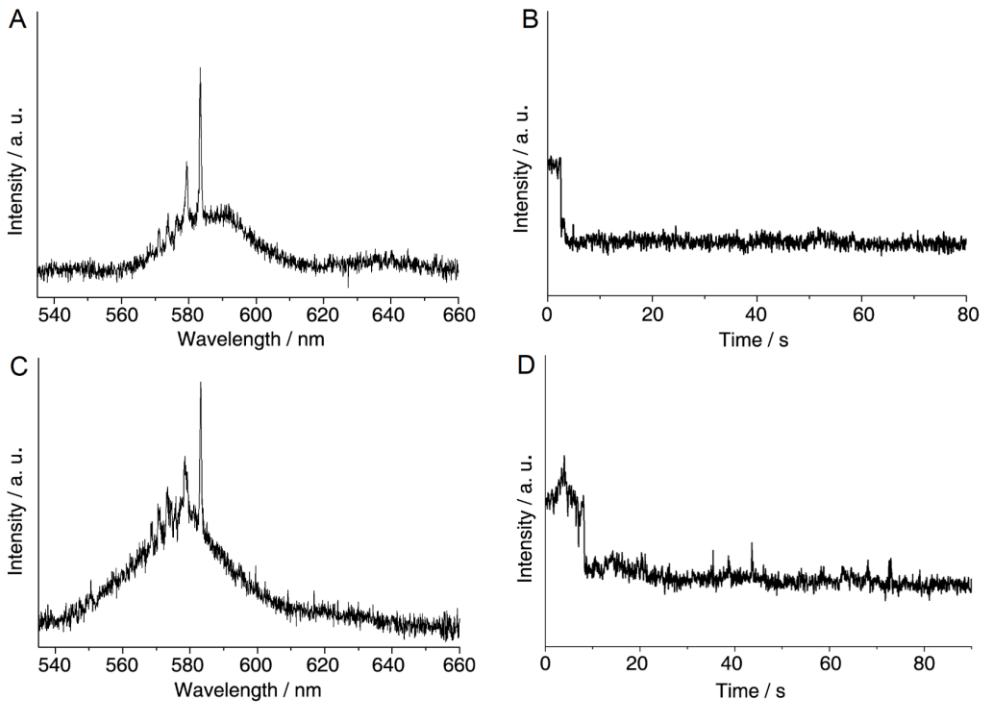

fig. S7. Two more representative SM spectra with Raman vibrational features. (**A**) and (**C**) Average SM emission spectra of RITC. (**B**) and (**D**) represent the corresponding emission intensity trajectories.

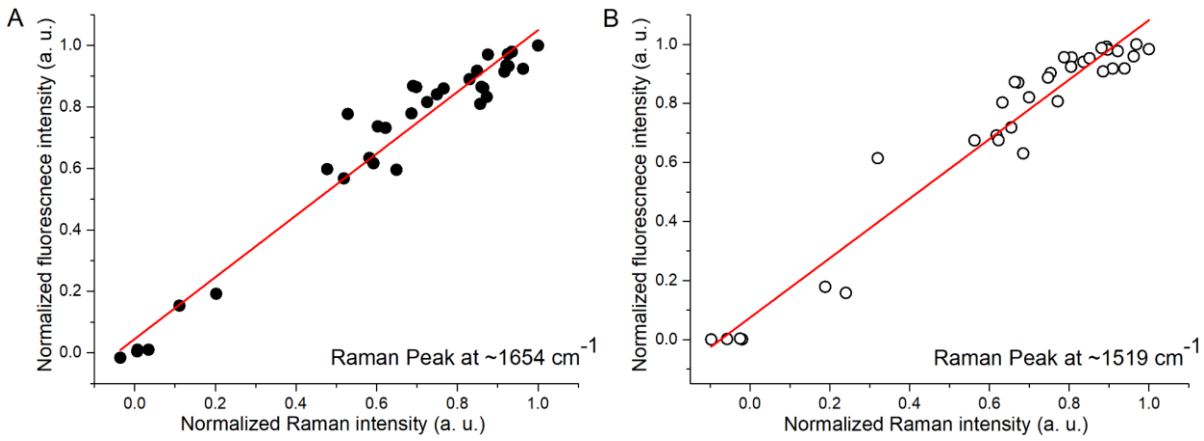

fig S8. Time-dependent intensity correlation between Raman peak and corresponding fluorescence background of the SM event shown in Fig. 3. (**A**) and (**B**) corresponds to Raman peaks at 1654 and 1519 cm^{-1} shown in Fig. 3A. For a higher SNR, each data point corresponds to an accumulation of 10 spectra and the red lines represent the linear fit.

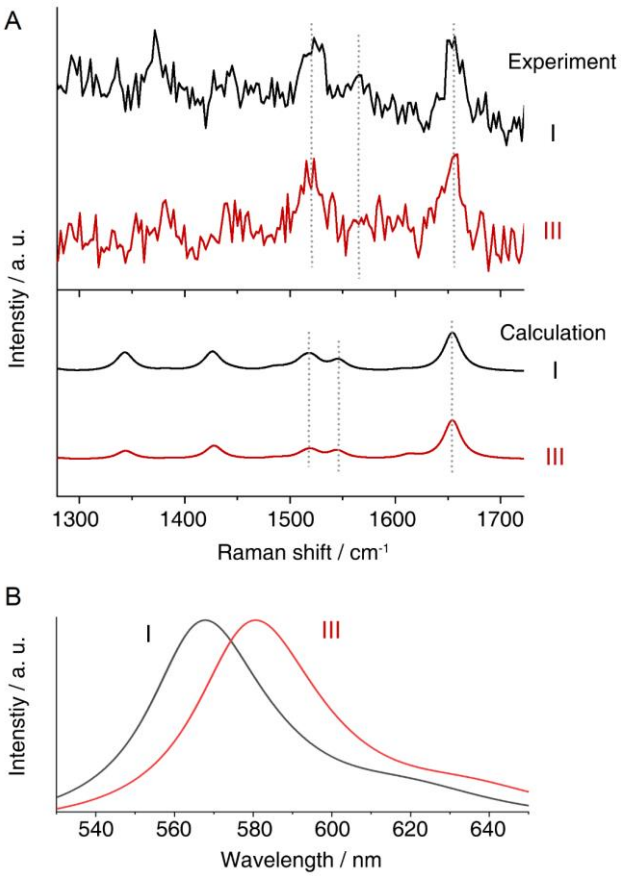

fig. S9. DFT calculations of Raman and fluorescence spectra of compounds I and III. (**A**) Experimental and calculated resonant Raman features of structure I and III. (**B**) Calculated fluorescence spectra of compounds I and III.

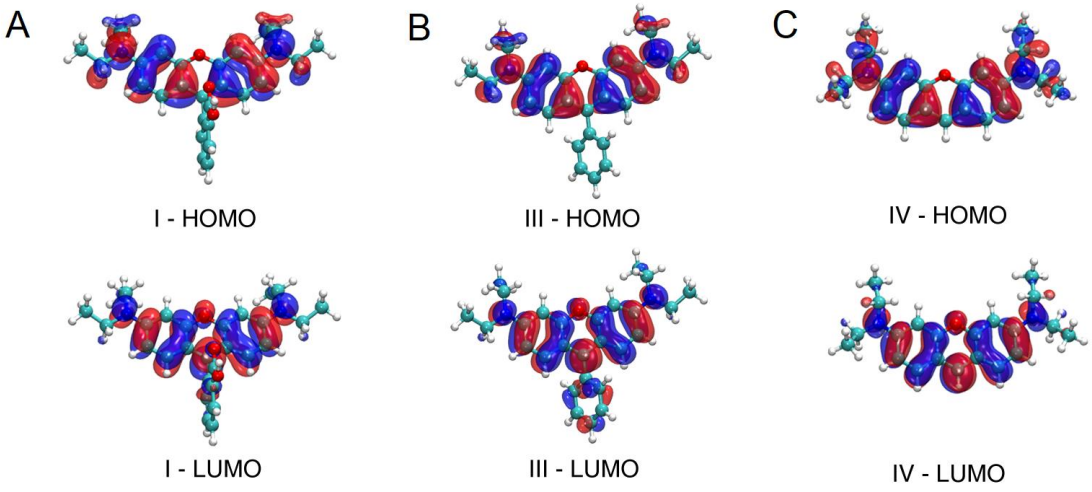

fig. S10. Molecular orbitals for structure I (A), III (B), and IV (C).

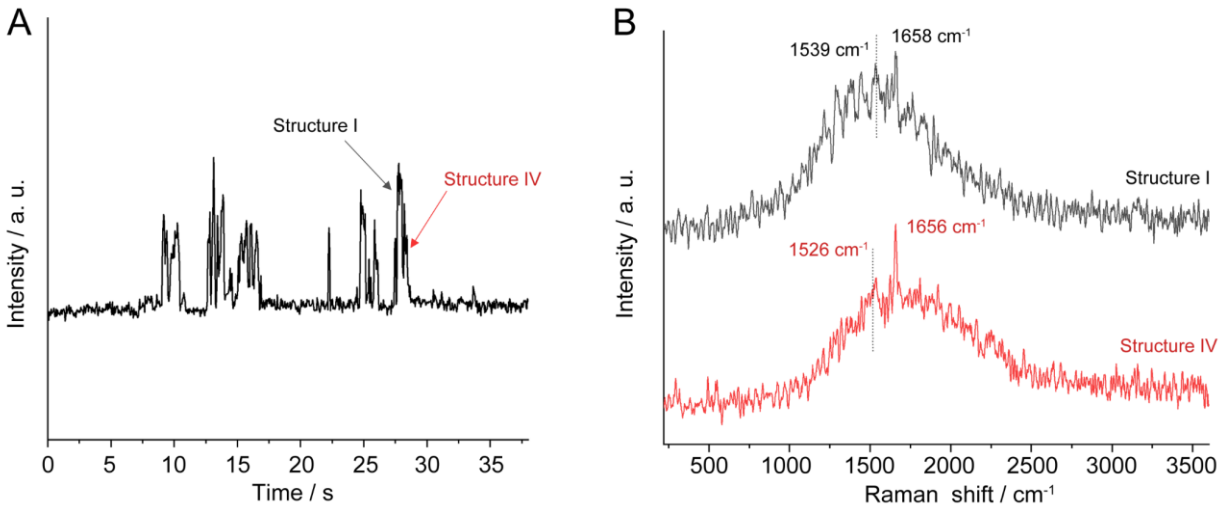

fig. S11. Reproducibility of SM study of photo-induced cleavage reaction of a single RITC molecule. (**A**) Emission intensity trajectory of a single RITC, where the spectral acquisition time is 50 ms. (**B**) Average spectra of single-molecule spectroscopy of RTIC during ~27.4-27.75 (structure I) and 28-28.4 s (structure IV). These spectra represent the structural transformation of structure I to IV, which corresponds to the time-dependent intensity changes denoted by the arrows in (A). For a higher SNR, a Savitzky-Golay smooth was applied to the spectra.

REFERENCES AND NOTES

1. S. M. Nie, D. T. Chiu, R. N. Zare, Probing individual molecules with confocal fluorescence microscopy. *Science* **266**, 1018–1021 (1994).

2. W. E. Moerner, M. Orrit, Illuminating single molecules in condensed matter. *Science* **283**, 1670–1676 (1999).

3. E. Betzig, G. H. Patterson, R. Sougrat, O. W. Lindwasser, S. Olenych, J. S. Bonifacino, M. W. Davidson, J. Lippincott-Schwartz, H. F. Hess, Imaging intracellular fluorescent proteins at nanometer resolution. *Science* **313**, 1642–1645 (2006).

4. R. Zhang, Y. Zhang, Z. C. Dong, S. Jiang, C. Zhang, L. G. Chen, L. Zhang, Y. Liao, J. Aizpurua, Y. Luo, J. L. Yang, J. G. Hou, Chemical mapping of a single molecule by plasmon-enhanced Raman scattering. *Nature* **498**, 82–86 (2013).

5. R. Chikkaraddy, B. de Nijs, F. Benz, S. J. Barrow, O. A. Scherman, E. Rosta, A. Demetriadou, P. Fox, O. Hess, J. J. Baumberg, Single-molecule strong coupling at room temperature in plasmonic nanocavities. *Nature* **535**, 127–130 (2016).

6. H. P. Lu, X. S. Xie, Single-molecule spectral fluctuations at room temperature. *Nature* **385**, 143–146 (1997).

7. F. Tenopala-Carmona, S. Fronk, G. C. Bazan, I. D. W. Samuel, J. C. Penedo, Real-time observation of conformational switching in single conjugated polymer chains. *Sci. Adv.* **4**, eaao5786 (2018).

8. J. B. Sambur, T. Y. Chen, E. Choudhary, G. Chen, E. J. Nissen, E. M. Thomas, N. Zou, P. Chen, Sub-particle reaction and photocurrent mapping to optimize catalyst-modified photoanodes. *Nature* **530**, 77–80 (2016).

9. T. Chen, B. Dong, K. Chen, F. Zhao, X. Cheng, C. Ma, S. Lee, P. Zhang, S. H. Kang, J. W. Ha, W. Xu, N. Fang, Optical super-resolution imaging of surface reactions. *Chem. Rev.* **117**, 7510–7537 (2017).

10. M. B. J. Roeffaers, B. F. Sels, H. Uji-I, F. C. De Schryver, P. A. Jacobs, D. E. De Vos, J. Hofkens, Spatially resolved observation of crystal-face-dependent catalysis by single turnover counting. *Nature* **439**, 572–575 (2006).

11. J. Guan, C. Jia, Y. Li, Z. Liu, J. Wang, Z. Yang, C. Gu, D. Su, K. N. Houk, D. Zhang, X. Guo, Direct single-molecule dynamic detection of chemical reactions. *Sci. Adv.* **4**, eaar2177 (2018).

12. B. Dong, Y. Pei, F. Zhao, T. W. Goh, Z. Qi, C. Xiao, K. Chen, W. Huang, N. Fang, Y. Pei, F. Zhao, T. W. Goh, Z. Qi, C. Xiao, K. Chen, W. Huang, N. Fang, In situ quantitative single-molecule study of dynamic catalytic processes in nanoconfinement. *Nat. Catal.* **1**, 135–140 (2018).

13. W. E. Moerner, D. P. Fromm, Methods of single-molecule fluorescence spectroscopy and microscopy. *Rev. Sci. Instrum.* **74**, 3597–3619 (2003).

14. J. Lakowicz, *Principles of fluorescence spectroscopy* (Springer, ed. 3, 2006).

15. G. P. Acuna, F. M. Möller, P. Holzmeister, S. Beater, B. Lalkens, P. Tinnefeld, Fluorescence enhancement at docking sites of DNA-directed self-assembled nanoantennas. *Science* **338**, 506–510 (2012).

16. E. M. van Schrojenstein Lantman, T. Deckert-Gaudig, A. J. G. Mank, V. Deckert, B. M. Weckhuysen, Catalytic processes monitored at the nanoscale with tip-enhanced Raman spectroscopy. *Nat. Nanotechnol.* **7**, 583–586 (2012).

17. T. Itoh, Y. S. Yamamoto, Y. Ozaki, Plasmon-enhanced spectroscopy of absorption and spontaneous emissions explained using cavity quantum optics. *Chem. Soc. Rev.* **46**, 3904–3921 (2017).

18. W. Xie, S. Schlücker, Hot electron-induced reduction of small molecules on photorecycling metal surfaces. *Nat. Commun.* **6**, 7570 (2015).

19. Y. C. Cao, R. Jin, C. A. Mirkin, Nanoparticles with Raman spectroscopic fingerprints for DNA and RNA detection. *Science* **297**, 1536–1540 (2002).

20. S. M. Nie, S. R. Emory, Probing single molecules and single nanoparticles by surface-enhanced Raman scattering. *Science* **275**, 1102–1106 (1997).

21. K. Kneipp, Y. Wang, H. Kneipp, L. T. Perelman, I. Itzkan, R. R. Dasari, M. S. Feld, Single molecule detection using surface-enhanced Raman scattering (SERS). *Phys. Rev. Lett.* **78**, 1667–1670 (1997).

22. H. Xu, E. J. Bjerneld, M. Käll, L. Börjesson, Spectroscopy of single hemoglobin molecules by surface enhanced Raman scattering. *Phys. Rev. Lett.* **83**, 4357–4360 (1999).

23. J. Li, Y. F. Huang, Y. Ding, Z. L. Yang, S. B. Li, X. S. Zhou, F. R. Fan, W. Zhang, Z. Y. Zhou, D. Y. Wu, B. Ren, Z. L. Wang, Z. Q. Tian, Shell-isolated nanoparticle-enhanced Raman spectroscopy. *Nature* **464**, 392–395 (2010).

24. C. Y. Li, M. Meng, S. C. Huang, L. Li, S. R. Huang, S. Chen, L. Y. Meng, R. Panneerselvam, S. J. Zhang, B. Ren, Z. L. Yang, J. F. Li, Z. Q. Tian, "Smart" Ag nanostructures for plasmon-enhanced spectroscopies. *J. Am. Chem. Soc.* **137**, 13784–13787 (2015).

25. A. Kinkhabwala, Z. Yu, S. Fan, Y. Avlasevich, K. Müllen, W. E. Moerner, Large single-molecule fluorescence enhancements produced by a bowtie nanoantenna. *Nat. Photonics* **3**, 654–657 (2009).

26. T. Vosgröne, A. J. Meixner, Surface- and resonance-enhanced micro-Raman spectroscopy of xanthene dyes: From the ensemble to single molecules. *ChemPhysChem* **6**, 154–163 (2005).

27. C. M. Galloway, P. G. Etchegoin, E. C. Le Ru, Ultrafast nonradiative decay rates on metallic surfaces by comparing surface-enhanced Raman and fluorescence signals of single molecules. *Phys. Rev. Lett.* **103**, 063003 (2009).

28. M. J. Walter, J. M. Lupton, K. Becker, J. Feldmann, G. Gaefke, S. Höger, Simultaneous Raman and fluorescence spectroscopy of single conjugated polymer chains. *Phys. Rev. Lett.* **98**, 137401 (2007).

29. M. Moskovits, Surface-enhanced spectroscopy. *Rev. Mod. Phys.* **57**, 783–826 (1985).

30. G. M. Akselrod, C. Argyropoulos, T. B. Hoang, C. Ciracì, C. Fang, J. Huang, D. R. Smith, M. H. Mikkelsen, Probing the mechanisms of large Purcell enhancement in plasmonic nanoantennas. *Nat. Photonics* **8**, 835–840 (2014).

31. N. J. Turro, V. Ramamurthy, J. C. Scaiano, *Modern Molecular Photochemistry of Organic Molecules* (University Science Books, 2010).

32. I. L. Arbeloa, K. K. Rohatgimukherjee, Solvent effect on photophysics of the molecular forms of rhodamine B: Solvation models and spectroscopic parameters. *Chem. Phys. Lett.* **128**, 474–479 (1986).

33. X. Hu, T. Mohamood, W. Ma, C. Chen, J. Zhao, Oxidative decomposition of rhodamine B dye in the presence of VO^{2+} and/or Pt(IV) under visible light irradiation: *N*-deethylation, chromophore cleavage, and mineralization. *J. Phys. Chem. B* **110**, 26012–26018 (2006).

34. P. Wilhelm, D. Stephan, Photodegradation of rhodamine B in aqueous solution via SiO_2@TiO_2 nano-spheres. *J. Photochem. Photobiol. A* **185**, 19–25 (2007).

35. P. Štacko, P. Šebej, A. T. Veetil, P. Klán, Carbon–carbon bond cleavage in fluorescent pyronin analogues induced by yellow light. *Org. Lett.* **14**, 4918–4921 (2012).

36. X. Luo, L. Qian, Y. Xiao, Y. Tang, Y. Zhao, X. Wang, L. Gu, Z. Lei, J. Bao, J. Wu, T. He, F. Hu, J. Zheng, H. Li, W. Zhu, L. Shao, X. Dong, D. Chen, X. Qian, Y. Yang, A diversity-oriented rhodamine library for wide-spectrum bactericidal agents with low inducible resistance against resistant pathogens. *Nat. Commun.* **10**, 258 (2019).

37. A. C. Aragonès, N. L. Haworth, N. Darwish, S. Ciampi, N. J. Bloomfield, G. G. Wallace, I. Diez-Perez, M. L. Coote, Electrostatic catalysis of a Diels–Alder reaction. *Nature* **531**, 88–91 (2016).

38. E. D. Palik, *Handbook of Optical Constants of Solids* (Academic Press, 1998), vol. 3.

39. A. Rose, T. B. Hoang, F. McGuire, J. J. Mock, C. Ciracì, D. R. Smith, M. H. Mikkelsen, Control of radiative processes using tunable plasmonic nanopatch antennas. *Nano Lett.* **14**, 4797–4802 (2014).

40. L. Novotny, B. Hecht, *Principles of Nano-Optics* (Cambridge Univ. Press, 2012).

41. P. J. Stephens, F. J. Devlin, C. F. Chabalowski, M. J. Frisch, *Ab initio* calculation of vibrational absorption and circular dichroism spectra using density functional force fields. *J. Phys. Chem.* **98**, 11623–11627 (1994).

42. R. Ditchfield, W. J. Hehre, J. A. Pople, Self-consistent molecular-orbital methods. IX. An extended Gaussian-type basis for molecular-orbital studies of organic molecules. *J. Chem. Phys.* **54**, 724–728 (1971).

43. F. Lipparini, G. Scalmani, B. Mennucci, E. Cancès, M. Caricato, M. J. Frisch, A variational formulation of the polarizable continuum model. *J. Chem. Phys.* **133**, 014106 (2010).

44. I. M. Alecu, J. Zheng, Y. Zhao, D. G. Truhlar, Computational thermochemistry: Scale factor databases and scale factors for vibrational frequencies obtained from electronic model chemistries. *J. Chem. Theory Comput.* **6**, 2872–2887 (2010).

45. P. Macak, Y. Luo, H. Ågren, Simulations of vibronic profiles in two-photon absorption. *Chem. Phys. Lett.* **330**, 447–456 (2000).

46. R. Bauernschmitt, R. Ahlrichs, Treatment of electronic excitations within the adiabatic approximation of time dependent density functional theory. *Chem. Phys. Lett.* **256**, 454–464 (1996).

47. Y.-J. Ai, F. Zhang, S.-F. Chen, Y. Luo, W.-H. Fang, Importance of the intramolecular hydrogen bond on the photochemistry of anionic hydroquinone (FADH−) in DNA photolyase. *J. Phys. Chem. Lett.* **1**, 743–747 (2010).

48. G. Tian, D. Sun, Y. Zhang, X. Yu, Franck–Condon blockade and aggregation-modulated conductance in molecular devices using aggregation-induced emission-active molecules. *Angew. Chem. Int. Ed.* **58**, 5951–5955 (2019).

49. G. T. Hermanson, *Bioconjugate Techniques* (Academic Press, 2013).

50. N. Rathor, S. Panda, Aminosilane densities on nanotextured silicon. *Mater. Sci. Eng. C* **29**, 2340–2345 (2009).